# Time Domain Wave Packet method and suppression of instability waves in aeroacoustic computations

## Fang Q. Hu

Department of Mathematics and Statitics

Old Dominion University, Norfolk, Virginia 23529

Email: fhu@odu.edu

X. D. Li, X. Y. Li and M. Jiang

School of Jet Propulsion

Beihang University, Beijing 100191, China

Email: lixd@buaa.edu.cn, lixiaoyan2001@googlemail.com, jm3304420@sjp.buaa.edu.cn

#### **ABSTRACT**

A new time domain methodology for Computational Aeroacoustics (CAA) is proposed. The Time Domain Wave Packet (TDWP) method employs a temporally compact broadband pulse for acoustic sources. As the radiation and transmission of acoustic waves of all frequencies within the numerical resolution are embedded in the propagation of the wave packet, acoustic solution of the full spectrum become available at once. In addition, it becomes possible to separate the acoustic and instability waves in shear flows in the Time Domain Wave Packet method due to the compactness of the wave packet. The instability waves can further be suppressed by a source filtering technique, applied after the acoustic wave packet has propagated through the shear layers. Details on the source filtering technique used in the paper are presented. The TDWP method has been validated using a CAA Benchmark problem. The TDWP method is also applied to the NASA/GE Fan Noise Source Diagnostic Test (SDT) exhaust radiation problem.

#### 1 Introduction

With the current computational power, it is not yet feasible to compute directly the generation and propagation of noise in an unsteady flow for most realistic aeroacoustics problems. A common approach in Computational Aeroacoustics (CAA) is to first carry out a steady RANS (Reynolds Averaged Navier-Stokes) type simulation and then, using the steady result as a base flow, compute the acoustic wave radiation and transmission with modeled noise sources [1]. The latter is done by solving linearized equations, often the linearized Euler equations. Although the absolute levels of noise are difficult to calculate in this approach, it nonetheless provides a very efficient and useful way to assess the effects of geometry, shape and flow condition on the noise propagation and directivity.

In many noise prediction problems, it is important to include the effects of mean flow shear layers on sound propagation. A well-known problem in solving the linearized Euler equations for the propagation of acoustic waves is the existence of intrinsic hydrodynamic instability waves in shear flows and its interference with the acoustic calculation. Whenever a shear flow whose velocity profile has an inflection point is present, a hydrodynamic instability wave, known as the Kelvin-Helmholtz instability wave, could be excited. The instability wave grows exponentially and can sometimes overwhelm the acoustic waves and complicate the boundary treatments. In some cases, its magnitude can become so large as to make the computation impossible. The larger the velocity gradient of the shear flow, the more persistent the problem. This instability wave problem is common in a wide range of aeroacoustics applications, such as in acoustic mode transmission in turbo-machinery, noise propagation through fan exhaust shear layers, liner treatment with grazing flows, etc.

One way to avoid the Kelvin-Helmholtz instability wave has been to solve the linearized Euler equations in the frequency domain [2–4]. However, for the frequency domain approach to be effective, it has been found to be necessary to solve the resultant linear system by a direct algebraic solver. This could be impractical when the number of unknowns becomes large, especially for three-dimensional problems.

The Kelvin-Helmholtz shear flow instability is of vortical nature. If the mean flow is uniform, it is well-known that the acoustic and vortical waves of the linearized Euler equations can be separated analytically, resulting in a single second-order wave equation for the acoustic pressure or density. When the mean flow is nonuniform, or when the medium of wave propagation is non-homogeneous, it becomes difficult to get a single equation just for the acoustic waves that excludes the vortical waves. To do so, often certain approximations are necessary [5–7]. In [6], an approximate wave equation is derived for the pressure when the medium density is non-constant. In [7], the Acoustic Perturbation Equations (APE) are derived, in which the vorticity solutions are filtered out in the derivation process.

As the vortical instability waves are difficult to be excluded analytically from the governing equations, one

alternative is to suppress the instability waves computationally. Mathematically, the Kelvin-Helmholtz instability wave is due to the existence of an inflection point in the mean streamwise velocity profile. A frequently used tactic of suppressing the instability wave in linear aeroacoustic calculations is to simply remove the velocity gradient terms in the linear governing equation [8]. This approach will be referred to as the Mean Flow Gradient Removal (MFGR) method. Another way of suppressing the instability is the Source Filtering (SF) technique, in which additional terms are added to the linear Euler equations so that the modified equations have a much reduced instability wave [9]. In the present work, the source filtering technique is pursued and new models are proposed that can be used to suppress the instability waves of the linearized Euler equations.

The present paper also takes a fresh look at the time domain approaches in Computational Aeroacoustics (CAA). A new methodology referred to as the Time Domain Wave Packet (TDWP) method is proposed. It differs from the more conventional approach in that the source time function will now be modeled by a temporally compact broadband pulse. In conventional time domain linear aeroacoustics computations, the acoustic sources, such as the point sources or incoming wave modes, are often specified as sinusoidal functions in time with a fixed frequency, or a group of frequencies, of interest. Then the time domain simulation is carried out until a time periodic state is reached. In the current TDWP method, the acoustic source will be modeled as a wave packet with a relatively short time duration. Under this setting, numerical simulation needs to last only until the wave packet has exited the computational domain, making it more efficient than the conventional time domain approach. More important, acoustic radiation and transmission at all frequencies within the numerical resolution are embedded in the propagation of the wave packet. As a result, by a Fast Fourier Transform (FFT), solutions at **all frequencies** can be obtained in a single time domain simulation.

The TDWP method also benefits from the suppression of instability waves in acoustic simulations with shear flows. The acoustic and instability waves travel at different speeds, the former at the speed of sound and the latter at the convective speed of the mean flow [10,11]. Since a wave packet is temporally compact, it becomes possible to separate the acoustic and instability waves in the TDWP method. The acoustic wave packet would propagate through the shear flow in a short period of time and before the growth of the instability wave becomes significant. The instability wave suppression techniques may be applied after the wave packet has propagated through the shear layer. In this way, any adverse effects of the modifications made to the governing equations, by either the Mean Flow Gradient Removal technique or the Source Filtering technique, on the acoustic waves would be limited.

The rest of the paper is organized as follows. Modified Euler equations based on the source filtering technique are presented in section 2. Then, the TDWP method is proposed in section 3. Validation of our approach for instability wave suppression for a CAA Benchmark problem is given in section 4. An application of the TDWP

method and source filtering technique to the NASA/GE fan noise Source Diagnostic Test (SDT) exhaust radiation problem is presented in sections 5. Section 6 contains our conclusions.

### 2 Source Filtering Technique

In this paper, suppression of hydrodynamic instability wave will be done by a source filtering technique in which the linearized Euler equations are modified by an added source-like term. The source filtering term is designed to suppress the growth of the instability waves while having as little an effect on the linear acoustic waves as possible. Our proposed source filtering models are given in this section, for the two-dimensional rectangular coordinates. The models for the three-dimensional cylindrical coordinates are given in the Appendix.

In two space dimensions, the modified linearized Euler equations are of the form,

$$\frac{\partial \mathbf{u}}{\partial t} + A \frac{\partial \mathbf{u}}{\partial x} + B \frac{\partial \mathbf{u}}{\partial y} + C \mathbf{u} + \varepsilon F \mathbf{u} = \mathbf{S}$$
 (1)

where

$$\mathbf{u} = \begin{pmatrix} \rho \\ u \\ v \\ p \end{pmatrix}, A = \begin{pmatrix} u_0 & \rho_0 & 0 & 0 \\ 0 & u_0 & 0 & \frac{1}{\rho_0} \\ 0 & 0 & u_0 & 0 \\ 0 & \gamma p_0 & 0 & u_0 \end{pmatrix}, B = \begin{pmatrix} v_0 & 0 & \rho_0 & 0 \\ 0 & v_0 & 0 & 0 \\ 0 & 0 & v_0 & \frac{1}{\rho_0} \\ 0 & 0 & \gamma p_0 & v_0 \end{pmatrix}, \tag{2}$$

$$C = \begin{pmatrix} \nabla \cdot \mathbf{u_0} & \frac{\partial \rho_0}{\partial x} & \frac{\partial \rho_0}{\partial y} & 0 \\ 0 & \frac{\partial u_0}{\partial x} & \frac{\partial u_0}{\partial y} & 0 \\ 0 & \frac{\partial v_0}{\partial x} & \frac{\partial v_0}{\partial y} & 0 \\ 0 & 0 & 0 & \gamma \nabla \cdot \mathbf{u_0} \end{pmatrix}$$

and the added *source filtering matrix* F is as follows,

$$F = \begin{pmatrix} 0 & 0 & 0 & 0 \\ 0 & 0 & -\alpha \frac{\partial u_0}{\partial y} & 0 \\ 0 & 0 & \beta \left| \frac{\partial u_0}{\partial y} \right| G(y) & 0 \\ 0 & 0 & 0 & 0 \end{pmatrix}, \quad G(y) = 1 - \frac{\left| \partial^2 u_0 / \partial y^2 \right|}{\left| \partial^2 u_0 / \partial y^2 \right|_{max}}$$
(3)

In the above,  $\rho$  is the density, p is the pressure, u and v are the velocities in the x and y directions respectively. A subscript 0 has been used to denote the mean state values.

When the mean velocity profile  $u_0$  has an inflection point, the term  $\frac{\partial u_0}{\partial y}$  in matrix C is responsible for the Kelvin-Helmholtz instability wave. A simple and frequently used tactic to void the instability waves is to remove this term from matrix C. This approach will be referred to as the Mean Flow Gradient Removal (MFGR) method in this paper. The removal of  $\frac{\partial u_0}{\partial y}$  in matrix C would inevitably affect the accuracy on the acoustic wave propagation. Instead of simply removing the velocity gradient, in the Source Filtering (SF) technique formulated in (1), an additional source-like term is introduced by matrix F. Here  $\alpha$  and  $\beta$  in (3) are the parameters in the source filtering model, and  $\varepsilon$  is a parameter that controls the strength of source filtering. While the  $\alpha$  term in (3) has the effect of directly reducing the streamwise velocity gradient term in matrix C, the  $\beta$  term is introduced with the intention of reducing the vorticity in the momentum equation. A linear stability analysis has been carried out which indicated that inclusion of the  $\beta$  term reduced the growth rate of the Kelvin-Helmholtz instability wave mode. The G(y)factor is included so that the β term is the largest near the inflection points of the mean velocity profile. In particular, when  $\varepsilon=1$ ,  $\alpha=1$  and  $\beta=0$ , the Mean Flow Gradient Removal model is obtained. When  $\varepsilon=0$ , the linearized Euler equation is recovered. The optimal values for  $\alpha$  and  $\beta$  for a given problem may be determined empirically. However, when the suppression technique is coupled with the TDWP method shown below, adverse effects of the  $\alpha$  and  $\beta$  terms on the acoustic waves are not expected to be significant. The source-filtering model for the linearized Euler equations in three-dimensional cylindrical coordinates is given in the Appendix.

#### 3 Time Domain Wave Packet (TDWP) method

In most time domain calculations in CAA, the acoustic sources are often modeled by a sinusoidal function in time with a specified frequency, or a group of frequencies, of interest. The numerical simulation is then carried out to reach a time periodic state. In the TDWP method proposed in this work, the time function for an acoustic source will instead be a temporally compact pulse, dubbed "Broadband Acoustic Test Pulse". It is short in time

duration and broad in its frequency spectrum. Such a source will generate a wave packet that contains a broad range of frequencies, as illustrated in Figure 1. For linear problems, wave propagation properties at all frequencies are embedded in the propagation of the wave packet. Therefore, radiation and scattering of acoustic waves at **all frequencies** within the numerical resolution can be obtained in a single Time Domain Wave Packet simulation. The FFT of the TDWP solution effectively yields the *acoustic transfer function* in the frequency domain. In addition, the Broadband Acoustic Test Pulse, as given below, has a short time duration, making the calculation more efficient than that of driving a single frequency solution to a time periodic state.

To generate a broadband wave packet, a time function with a wide spectrum is to be used for the source. In our work, we use a simple time function defined as

$$\Psi(t) = \begin{cases} \frac{\Delta t \sin(\omega_0 t)}{\pi t} e^{(\ln \delta)(t/M\Delta t)^2} |t| \le M\Delta t \\ 0 |t| > M\Delta t \end{cases}$$
(4)

where  $\Delta t$  is the time step in the time domain simulation,  $\delta$  is a small number, and M and  $\omega_0$  are adjustable parameters of the function. This source function is non-zero only for a limited time duration,  $-M\Delta t \leq t \leq M\Delta t$ , while its spectrum is broadband and covers frequencies up to slightly beyond  $\omega_0$ . More sophisticated time and frequency band-limited functions can also be used (see, e.g., [12]).

An example of  $\Psi(t)$  is plotted in Figure 2 where the parameters are M=40,  $\omega_0 \Delta t = \pi/4$  and  $\delta=0.01$ . For the case shown in Figure 2, the acoustic source term will be active for only 80 time steps, while all waves with a period as small as  $4\Delta t$ , or a frequency as large as  $1/4\Delta t$ , are included in the computation.

Compared to single frequency source functions, use of a wave packet has several advantages, including: (1) One computation for all frequencies within numerical resolution; (2) A very short time duration at the source; (3) Possibility of separation of acoustic and instability waves; (4) Ability to synthesize broadband noise source.

An added benefit of the TDWP method is that it becomes possible for the separation of acoustic and instability waves in the shear flow, as these two kinds of waves travel at different speeds [10,11]. This makes it possible to apply the instability suppression technique, presented in section 2, after the separation of instability and acoustic waves. In such cases, any adverse effect of modified linearized Euler equations, designed for the suppression of instability waves, on the acoustic waves can be further made minimal.

#### 4 A CAA Benchmark problem

The source filtering technique, coupled with the TDWP method, will be first applied to a shear layer acoustic radiation problem, a CAA Benchmark Workshop problem [13]. In this problem, the mean flow is given as follows:

$$u_0(y) = \begin{cases} u_j e^{-(\ln 2)(|y|/b - h/b)^2} & |y| > h \\ u_j & |y| \le h \end{cases}$$
 (5)

$$\frac{1}{\rho_0(y)} = -\frac{1}{2} \frac{\gamma - 1}{\rho_j a_j^2} (u_0(y) - u_j) u_0(y) + \frac{1}{\rho_j} \frac{u_0(y)}{u_j} + \frac{1}{\rho_\infty} \frac{u_j - u_0(y)}{u_j}$$
(6)

$$\rho_{\infty}/\rho_j = 2$$
,  $u_j/a_j = 0.756$ ,  $b = 1.3$ ,  $h = 0$ 

where  $u_j$ ,  $\rho_j$  and  $a_j$  denote the mean velocity, density and speed of sound at jet centerline. Further details on the problem are referred to [13].

#### 4.1 Single frequency simulation without source filtering

In the Benchmark problem, an acoustic source is placed inside the jet. The source is specified as a sinusoidal forcing term in the pressure equation in (1) of the form

$$S(x, y, t) = \sin(\Omega t) e^{-(\ln 2)(B_x x^2 + B_y y^2)}$$
(7)

where  $\Omega = 76 \text{(rad/s)}$  and  $B_x = 0.32$ ,  $B_y = 0.04$ .

Instantaneous pressure contours of a direct simulation of the linearized Euler equations without the source filtering term (equation (1) with  $\varepsilon=0$ ) is shown in Figure 3 (left). The Kelvin-Helmholtz instability wave is excited and grows exponentially downstream. This instability wave clearly would interfere with the near-field acoustic solutions. It can also cause problems at the outflow nonreflecting boundary for the linear acoustic calculations

when the amplitude of the instability wave becomes exceedingly large.

#### 4.2 TDWP simulation

To carry out the computation by the TDWP method, the sinusoidal pressure source term given by (7) will now be replaced by a wave packet forcing term as follows:

$$S_{TDWP}(x, y, t) = \Psi(t)e^{-(\ln 2)(B_x x^2 + B_y y^2)}$$
(8)

where  $\Psi(t)$  is that given in (4). Such a source term will generate a wave packet with a broad spectrum as shown in Figure 2.

The wave packet propagates through the shear flow and to the far field. A time history of pressure contours by the TDWP method is shown in Figure 4. On the left of Figure 4, direct simulation of the Euler equations without instability suppression is shown. As noted earlier, due to the fact that the acoustic and instability waves travel in different speeds, the propagation of the acoustic wave packet becomes separated from that of the instability wave. Mean flow effects on the acoustic wave propagation for all frequencies are embedded in the evolution of the acoustic wave packet.

On the right of Figure 4, simulation of linearized Euler equation by the TDWP method and with the source filtering term is shown. To minimize the effects of the source filtering term on the acoustic wave packet, the source filtering is turned on slowly with the parameter  $\varepsilon$  in (17) given as below:

$$\varepsilon = \begin{cases} 0 & t \le t_0 \\ 1 - e^{-(\ln 2)(t - t_0)^2/\tau^2} & t > t_0 \end{cases}$$
 (9)

The source filtering is turned on after  $t_0$ , an estimated time by which the pulse has propagated through of the shear layer. For the calculations shown here,  $t_0 = 10$  and  $\tau = 30$ . As the instability wave starts slowly, numerical solution is not expected to be very sensitive to the specific form of the  $\varepsilon$  shown in (9). For this example, the parameters used in the source filtering technique are  $\alpha = 0.25$  and  $\beta = 0.75$ .

The wave packet entails the propagation properties of acoustic waves at all frequencies. By an FFT, the frequency domain solutions can be obtained readily. The pressure contours obtained by FFT of the TDWP solution

at frequency  $\Omega$  as specified in (7) are shown in Figure 3 (right), exhibiting similarity to those of the acoustic waves by the original Euler equations shown in the figure on the left. Figure 5 shows the pressure distributions along y = 15, 50 and x = 100, and their comparisons with the analytic solutions, with very good agreements. The TDWP method would be even more efficient than the single frequency sinusoidal wave approach when solutions at multiple frequencies are required.

## 5 Application to SDT aft fan radiation

In this section, the source filtering technique and the TDWP method will be applied to the NASA/GE fan noise Source Diagnostic Test (SDT) exhaust radiation problem [14–18]. The flow path of the SDT fan as well as the mean flow Mach number inside the duct are sketched in Figure 6.

To predict aft fan noise, it is important to include the effects of the exhaust shear flow on the radiation of fan tonal and broadband noises [14, 16, 19–23]. On the other hand, the growth of Kelvin-Helmholtz instability wave of the exhaust shear flow may interfere with the computation of the linear acoustic waves. For aft fan exhaust radiation computation, in addition to the usual considerations on computational grids, spatial and temporal discretizations and nonreflecting boundary conditions that are common to most CAA problems, two important issues have to be addressed: (1) How to avoid the instability waves in the exhaust shear flow; (2) How to satisfactorily impose duct mode inflow condition.

Both issues can be dealt with by the techniques developed in the current paper. A schematic of the numerical simulation strategy is shown in Figure 7, with the nacelle, centerbody and shear layer of the exhaust flow. The wave packet for a selected duct mode is generated by using the broadband source term at a prescribed source plane inside the duct. Specifically, the source term for the pressure equation in (17) (Appendix) will now be given by

$$S_{TDWP}(x, r, \theta, t) = \Psi(t)\phi_{mn}(r)e^{-(\ln 2)(x - x_s)^2/b^2}e^{im\theta}$$
(10)

where  $\phi_{mn}(r)$  is the eigenfunction (mode shape) of the (m,n) mode that is to be simulated, in which m and n are the azimuthal and radial mode indices respectively. This source function is used to generate a wave packet for the (m,n) mode inside the duct. Of course a combination of multiple modes may also be used for a desired source composition. Alternatively, results for various combinations of multiple modes can be synthesized using multiple single mode simulations. Here  $x_s$  denotes the location of the source plane inside the duct and b is the half-width of the source region. The wave packet entails the wave mode (m,n) at all frequencies. Since the mean flow is

assumed to be locally uniform around the source plane, mode shape  $\phi_{mn}(r)$  is independent of the frequency. Due to dispersive nature of the duct modes, waves with a higher frequency would arrive at the far-field sooner than those with a lower frequency. The acoustic waves will also trigger the hydrodynamic instability of the exhaust shear flow. The instability wave of the exhaust jet is to be suppressed by the source filtering technique. As the acoustic wave packet is separated from the instability waves in the time domain computation, application of the source filtering technique can be turned on after the wave packet has propagated through the shear layer. By an FFT of the time domain solution, propagation of the acoustic waves of all cut-on frequencies with the effects of mean flow included are obtained in one single computation.

## 5.1 Computational domain and duct mode dispersion relations

The computational domain and mesh used in the simulation are shown in Figure 8. Two body-fitted meshes are used. A finite difference scheme has been used to solve the linearized Euler equations (17) in the cylindrical coordinates [24, 25]. The spatial derivatives are approximated by the 7-point 4th-order central differences (DRP scheme) [25], and the time integration is carried out by 4th-order optimized Runge-Kutta scheme (LDDRK56) [24].

At all the non-reflecting boundaries, including the one that terminates the domain inside the duct, Perfectly Matched Layer (PML) absorbing boundary conditions are applied [26–28]. For a fixed azimuthal number m, we can assume the solution to be

$$11 - 11 - e^{im\theta}$$

The PML equations for the cylindrical coordinates (see (17) in appendix) are as follows [28],

$$\frac{\partial \mathbf{u}_{m}}{\partial t} + A \frac{\partial \mathbf{u}_{m}}{\partial x} + B \frac{\partial \mathbf{u}_{m}}{\partial r} + \frac{im}{r} C \mathbf{u}_{m} + \frac{1}{r} D \mathbf{u}_{m} + E \mathbf{u}_{m} + \varepsilon F \mathbf{u}_{m} + \sigma_{x} \mathbf{q}_{m}^{(1)} + \sigma_{r} \mathbf{q}_{m}^{(2)} + \frac{\bar{\sigma}_{r}}{r} \mathbf{q}_{m}^{(3)} + \sigma_{x} \bar{\beta} A \mathbf{u}_{m} = \mathbf{S}_{m}$$

$$(11)$$

$$\frac{\partial \mathbf{q}_{m}^{(1)}}{\partial t} + A \frac{\partial \mathbf{u}_{m}}{\partial x} + \sigma_{x} \mathbf{q}_{m}^{(1)} + \sigma_{x} \bar{\beta} A \mathbf{u}_{m} = 0$$
(12)

$$\frac{\partial \mathbf{q}_{m}^{(2)}}{\partial t} + B \frac{\partial \mathbf{u}_{m}}{\partial x} + \sigma_{r} \mathbf{q}_{m}^{(2)} = 0 \tag{13}$$

$$\frac{\partial \mathbf{q}_{m}^{(3)}}{\partial t} + \frac{im}{r} C \mathbf{u}_{m} + \frac{1}{r} D \mathbf{u}_{m} + \frac{\bar{\mathbf{\sigma}}_{r}}{r} \mathbf{q}_{m}^{(3)} = 0$$

$$\tag{14}$$

where the absorption coefficients are

$$\sigma_x = \sigma_{max} \left( \frac{x - x_0}{D} \right)^2, \quad \sigma_r = \sigma_{max} \left( \frac{r - r_0}{D} \right)^2, \quad \bar{\sigma}_r = \int_{r_0}^r \sigma_r dr$$

in which,  $x_0$  and  $r_0$  denotes the location of the Euler and PML interface for x- and r-layers respectively and D denotes the thickness of the absorbing domain. For the computations reported here, we use  $D=20\Delta x$  and  $\sigma_{max}=2/\Delta x$ . The auxiliary variable  $\mathbf{q}_{\mathbf{m}}^{(1)}$  is only required in the PML zones terminating the grids in the x direction (x-layers) and  $\mathbf{q}_{\mathbf{m}}^{(2)}$  and  $\mathbf{q}_{\mathbf{m}}^{(3)}$  are only required in the PML zones terminating the grid in the r direction (r-layers). The parameter  $\bar{\beta}$  in (11) and (12) is related to the space-time transformation used in deriving the PML equations [27]. Specifically,  $\bar{\beta} = \bar{u}_0/(1-\bar{u}_0^2)$  in which  $\bar{u}_0$  is the average mean axial velocity in the x-layer.

For the SDT geometry, the duct cross section area is non-uniform. For simplicity, the mean flow inside the duct has been approximated by a one-dimensional compressible flow. It is nonuniform only in the axial direction and is assumed to be locally uniform in the radial direction in our computation. For an approach condition of 7809 RPM (67.7% design speed), the variation of axial velocity along the nonuniform duct has been shown in Figure 6. For the jet exhaust flow outside the duct, the mean flow is obtained from a steady RANS (Reynolds Averaged Navier-Stokes) simulation. The RANS simulation was an axisymmetric solution from which the mean flow for the acoustic mesh was interpolated.

As the mean flow is axially nonuniform inside the duct, dispersion relations of duct modes would vary along the duct. By a local constant cross section assumption, it is well-known that the duct dispersion relation for mode (m,n) in an annular duct is determined by

$$k_{mn}^{\pm} = \frac{\pm \sqrt{(\omega^2 - (1 - M^2)\alpha_{mn}^2 - M\omega)}}{1 - M^2}$$

where  $\omega$  is the wave frequency, M is the mean flow Mach number which depends on the axial location,  $k_{mn}^{\pm}$  is the wave number of the right (+) and left (-) traveling modes respectively, and  $\alpha_{mn}$  is a root of

$$Y'_{m}(\alpha_{mn}h)J'_{m}(\alpha_{mn}) - J'_{m}(\alpha_{mn}h)Y'_{m}(\alpha_{mn}) = 0$$
(15)

in which  $J_m$  and  $Y_m$  are the Bessel functions of the first and second kinds of order m and h is the duct hub-to-tip ratio [18–20,22].

The SDT fan has a design of 22 blades and 54 exit guided vanes. The rotating fan and the static stator create the so-called Tyler-Sofrin interaction modes [29]. The azimuthal mode number of the interaction modes is determined by

$$m = nB + kV$$

where *B* is the number of blades of the fan and *V* is the number of stator vanes, and *n* and *k* are arbitrary integers. At 2BPF (Blade Passing Frequency), the first Tyler-Sofrin interaction mode has an azimuthal mode number m = -10.

We will report results for the m = -10 interaction mode. In the region close to and behind the exit guided vane, at a hub-to-tip ratio h = 0.529 and M = 0.35, the dispersion relations of the duct modes are plotted in Figure 9, left. At 2BPF of the approach condition (67.7% of the design speed and 7809 RPM), the first five modes are cut-on.

Downstream toward the duct exhaust, at a hub-to-tip ratio h = 0.609 and M = 0.4, the dispersion relations are plotted in Figure 9, right. Due to the variation in duct geometry, the fifth mode, (-10,4), becomes cut-off and, consequently, there are four cut-on modes at locations towards the duct exhaust.

## 5.2 Time Domain Wave Packet simulations

For each individual mode (m,n), a Time Domain Wave Packet simulation can be carried out, by specifying the source function given in (10) at a source plane close to a location behind the exit guided vanes, as sketched in Figure 7. This will generate a wave packet inside the duct of all the frequencies for the chosen mode. Waves with a cut-on frequency will propagate through the duct exhaust and to the far-field. The waves that propagate toward the nonreflecting boundary inside the duct will be absorbed and not reflected.

Due to the dispersive nature of the duct modes, as shown in the dispersion relations in Figure 9, waves with a higher frequency have a larger group velocity (slope of the dispersion curve) and thus will arrive at the far field sooner than waves with a lower frequency. A sample time history of pressure at a far field point is shown in Figure 10. The time signal shows higher frequencies at the beginning and oscillates with a lowered frequency as time increases. An FFT of the time signal, its magnitude given also in Figure 10, bottom, indicates that no cut-off frequency is present in the far field. This is consistent with the dispersion relations given in Figure 9. Figure 10 also shows that far field radiated sound pressure for all cut-on frequencies is available in a single TDWP

simulation.

In Figure 11, a sample pressure history at a point inside the shear flow is plotted when the time domain simulation is carried out with and without instability wave suppression. The exponential growth of the instability wave is apparent in the top Figure, without the instability suppression technique. It is also clearly shown that the acoustic wave packet, due to its compactness, is well separated from the instability wave in time. This implies that when the source filtering term is applied after the acoustic wave packet has propagated through the shear flow, the effect of the suppression on the acoustic wave packet will be minimal, as shown in the bottom Figure. While the instability waves are now suppressed, the acoustic wave packet remains the same as that in the top figure.

Near-field pressure distributions for the Source Diagnostic Test (SDT) aft fan radiation are shown in Figures 12-14, at 2BPF (Blade-Passing-Frequency) and for rotor-stator interaction modes (-10,0) to (-10,4). The frequency domain solutions are obtained by an FFT of the time domain solutions. The exhaust shear flow effects on the acoustic radiation are captured by the TDWP method, and the instability waves are suppressed successfully. We emphasize that solutions at other frequencies are also available in the same time domain simulation.

At all the nonreflecting boundaries, out-going waves are numerically absorbed by the PML without any visible reflection. For the (-10,4) mode shown in Figure 23, because the wave mode becomes cut-off near the duct exit, a large internal reflection occurs and the radiated sound is seen at a much lower level than that of cut-on modes as expected. This is generally consistent with an earlier study of SDT tonal noise in the frequency domain [30].

In the calculations for Figures 12-14, without applying the suppression technique, the instability wave was visible in the pressure contour plots. However, in this particular case of the SDT configuration, because of the rapid expansion of the jet shear layer as well as the short time duration of the wave packet, the instability wave did not grow as significantly as that seen in the benchmark problem in Figure 3. Numerical results at the far field obtained with the instability wave suppression technique were not found to be substantially different from those obtained without the suppression.

In the experimental studies of the SDT fan noise radiation problem, far field sound pressure levels were measured at a number of fixed locations [14]. A comparison between the far field results of the current computation and that of the experimental study will be presented next, for the case of approach condition of 7809 RPM (67.7% design speed) at 2BPF, where the m = -10 interaction mode is the dominant source [15]. The computational domain is extended to include the far field microphone locations of the experiment and, for each cut-on radial mode (n = 0 to 4), the far field pressure response is computed by the TDWP method. The far field pressure distribution with respect to the unit modal amplitude is obtained from the computation and denoted as  $P_n(\mathbf{r}, \omega)$ , where  $\mathbf{r}$  is the far field point and n is the radial mode number. Then the total far field pressure at point  $\mathbf{r}$  can be formed as

$$|P(\mathbf{r}, \mathbf{\omega})|^2 = \sum_{n=0}^4 |A_n|^2 |P_n(\mathbf{r}, \mathbf{\omega})|^2$$
(16)

In order to compare the computed far field pressure directivity with that of the experimental measurements, the magnitudes of the mode amplitudes  $|A_n|$  to be used in (16) are determined by a least squares fitting between the computed and the measured sound pressure level. Figure 15 shows a comparison of the computed and measured values for the exhaust radiation directions, where the modal power levels  $W_n$ , directly related to the amplitude of the radial modes  $A_n$  [31], are:  $W_0 = 97(dB)$ ,  $W_1 = 61(dB)$ ,  $W_2 = 86(dB)$ ,  $W_3 = 91(dB)$  and  $W_4 = 52(dB)$  (ref.  $10^{-12}$ Watts), with a relatively good agreement, especially in the main radiation direction.

The expression in (16) has assumed that the duct modes are not mutually interfering. Another computation has been conducted where both the magnitude and the phase of the mode amplitude were used in the least squares fitting. The results were, however, found to be similar to those given in Figure 15. These results indicate that the first radial mode has the largest contribution to the far field in this particular case.

We note that the proposed TDWP method is also applicable to the adjoint Euler equations. Further application of the TDWP method to the adjoint formulation for the open duct radiation problem as well as the reciprocal conditions between the forward and adjoint solutions can be found in reference [32].

## 6 Conclusions

An efficient and effective approach for linear time domain simulations, the Time Domain Wave Packet (TDWP) method, has been developed and demonstrated in this paper. Combined with the source filtering technique, the TDWP method can effectively avoid the instability wave through a separation of the acoustic wave packet and the instability wave, exploiting the fact that the two types of waves propagate at different speeds. The TDWP method is also generally more efficient than the conventional single frequency sinusoidal wave approach in time domain. Its ability to compute acoustic radiation at all frequencies in one time domain computation should be particularly useful for solving aeroacoustic problems involving broadband noise sources.

Application of the TDWP method to the NASA/GE fan noise Source Diagnostic Test (SDT) exhaust radiation problem shows that it is an effective method for duct acoustics, capable of imposing correctly a specified acoustic source mode inside the duct. The shear layer effects on fan noise radiation are captured accurately by a combination of the Source Filtering technique and the TDWP method.

The Time Domain Wave Packet method should also be applicable to cases with acoustically lined walls, with

the implementation of time domain impedance conditions. This will be investigated as a future work.

Acknowledgment: We thank the reviewers for their constructive comments and suggestions which are very helpful in improving the paper. This work is supported by the Aeroacoustics Research Consortium (AARC). The authors (X. D. Li, X. Y. Li and M. Jiang) were also partially supported by 973 program 2012CB720202 and 111 project-B07009 of China. We thank Dr. Edmane Envia of NASA Glenn Research Center for providing the SDT geometry and the associated RANS mean flow to one of the authors (FQH). This work used the Extreme Science and Engineering Discovery Environment (XSEDE), which is supported by National Science Foundation grant number OCI-1053575.

#### **Appendix**

The linearized Euler equations with source filtering term in cylindrical coordinates can be written as

$$\frac{\partial \mathbf{u}}{\partial t} + A \frac{\partial \mathbf{u}}{\partial x} + B \frac{\partial \mathbf{u}}{\partial r} + \frac{1}{r} C \frac{\partial \mathbf{u}}{\partial \theta} + \frac{1}{r} D \mathbf{u} + E \mathbf{u} + \varepsilon F \mathbf{u} = \mathbf{S}$$
(17)

where

$$\mathbf{u} = \begin{pmatrix} \rho \\ u \\ v \\ w \\ p \end{pmatrix}, A = \begin{pmatrix} u_0 & \rho_0 & 0 & 0 & 0 \\ 0 & u_0 & 0 & 0 & \frac{1}{\rho_0} \\ 0 & 0 & u_0 & 0 & 0 \\ 0 & 0 & 0 & u_0 & 0 \\ 0 & \gamma p_0 & 0 & 0 & u_0 \end{pmatrix}, B = \begin{pmatrix} v_0 & 0 & \rho_0 & 0 & 0 \\ 0 & v_0 & 0 & 0 & 0 \\ 0 & 0 & v_0 & 0 & \frac{1}{\rho_0} \\ 0 & 0 & 0 & v_0 & 0 \\ 0 & 0 & \gamma p_0 & 0 & v_0 \end{pmatrix},$$
(18)

$$E = \begin{pmatrix} \frac{\partial u_0}{\partial x} + \frac{\partial v_0}{\partial r} & \frac{\partial \rho_0}{\partial x} & \frac{\partial \rho_0}{\partial r} & 0 & 0 \\ -\frac{1}{\rho_0^2} & \frac{\partial \rho_0}{\partial x} & \frac{\partial u_0}{\partial x} & \frac{\partial u_0}{\partial r} & 0 & 0 \\ -\frac{1}{\rho_0^2} & \frac{\partial \rho_0}{\partial x} & \frac{\partial v_0}{\partial x} & \frac{\partial v_0}{\partial r} & 0 & 0 \\ 0 & 0 & 0 & 0 & 0 \\ 0 & \frac{\partial \rho_0}{\partial x} & \frac{\partial \rho_0}{\partial r} & 0 & \gamma(\frac{\partial u_0}{\partial x} + \frac{\partial v_0}{\partial r}) \end{pmatrix}$$

in which u, v and w are velocity components in the x, r and  $\theta$  directions respectively.

For equations in the cylindrical coordinates, the added source filtering matrix F is as follows,

Again,  $\varepsilon$  is a parameter that controls the strength of source filtering.

# References

[1] Panek, L., Schonwald, N., Richter, C., and Thiele, F., 2008, "Simulation of the rearward propagtion of fan noise through a long cowl aero-engine", *AIAA paper 2008-2820*.

- [2] Agarwal, A., Morris, P., and Mani, R., 2004, "The calculation of sound propagation in nonuniform flows: suppression of instability waves", AIAA Journal, **42**, pp. 80-88.
- [3] Casalino, D., and Genito, M., 2008, "Turbofan aft noise predictions based on lilley's wave model", AIAA Journal, **46**, pp. 84-93.
- [4] Iob, A., Arina, R., and Schipani, C., 2010, "Frequency-Domain linearized Euler model for turbomachinery noise radiation through engine exhaust", AIAA Journal, **48**, pp. 848-858.
- [5] Bergliaffa, S. E. P., Hibberd, K., Stone, M., and Visser, M., 2004, "Wave equation for sound in fluids with vorticity", Physica D, **191**, pp. 121-136.
- [6] Pierce, A. D., 1990, "Wave equation for the sound in fluids with unsteady inhomogeneous flow", Journal of Acoustical Society of America, **87**, pp. 2292-2299.
- [7] Ewert, R., and Schroder, R., 2003, "Acoustic perturbation equations based on flow decomposition via source filtering", Journal of Computational Physics, **188**, pp. 365-398.
- [8] Bogey, C., Bailly, A., and Juv'e, D., 2002, "Computation of flow noise using source terms in linearized Euler equations", AIAA Journal, **40**, pp. 235-243.
- [9] Li, X. D., Gao, J. H., Eschricht, D., and Thiele, F., 2004, "Numerical computation of the radiation and refraction of sound waves through a two dimensional shear layer", *NASA CP* 2004-212954, pp. 159-164.
- [10] Criminale, W. O., Jackson, T. L., and Joslin, R. D., 2003, *Theory and Computation of Hydrodynamic Stability*, Cambridge University Press.
- [11] Drazin, P. G., and Reid, W. H., 2004, *Hydrodynamic Stability*, Cambridge University Press.
- [12] Knab, J. J., 1979, "Interpolation of band-limited functions using the approximate prolate series", IEEE Transactions on Information Theory, **25**, pp. 717-720.
- [13] Dahl, M. D., ed., 2004, "Proceedings of Fourth Computational Aeroacoustics (CAA) Workshop on Benchmark Problems", *NASA CP* 2004-212954.
- [14] Envia, E., Tweedt, D. L., Woodward, R. P., Elliott, D. M., Fite, E. B., Hughes, C. E., Podboy, G. G., and Sutliff, D. L., 2008, "An assessment of current fan noise prediction capability", *AIAA paper 2008-2991*.
- [15] Heidelberg, L. J., 2002, "Fan noise source diagnostic test Tone Modal Structure Results", *NASA TM 2002-211594*.
- [16] Nark, D. M., Envia, E., and Burley, C. L., 2009, "Fan noise prediction with application to aircraft system noise assessment", *AIAA paper 2009-3291*.
- [17] Sharma, A., Richards, S. K., Woods, T. H., and Shieh, C., 2009, "Numerical prediction of exhaust fan-tone noise from high-bypass aircraft engines", AIAA Journal, **47**, pp. 2866-2878.
- [18] Sutliff, D. L., 2005, "Rotating rake turbofan duct mode measurement system", NASA TM 2005-213828.

- [19] Gabard, G., and Astley, R., 2006, "Theoretical model for sound radiation from annular jet pipes: far- and near-field solutions", Journal of Fluid Mechanics, **549**, pp. 315-341.
- [20] Meyer, H. D., and Envia, E., 1996, "Aeroacoustic analysis of turbofan noise generation", NASA CR 4715.
- [21] Richards, S. K., Chen, X. X., Huang, X., and Zhang, X., 2007, "Computation of fan noise radiation through an engine exhaust geometry with flow", International Journal of Aeroacoustics, **6**, pp. 223-241.
- [22] Rienstra, S. W., 1999, "Sound transmission in slowly varying circular and annular lined ducts with flow", Journal of Fluid Mechanics, **380**, pp. 279-296.
- [23] Zhang, X., and Chen, X., 2010, "Time-domain computation of multimode propagation in an aero-engine duct", Procedia Engineering, 6, pp. 173-182.
- [24] Hu, F. Q., Hussaini, M. Y., and Manthey, J. L., 1996, "Low-dissipation and low-dispersion Runge-Kutta schemes for computational acoustics", Journal of Computational Physics, **124**, pp. 177-191.
- [25] Tam, C. K. W., and Webb, J. C., 1993, "Dispersion-relation-preserving finite difference schemes for computational acoustics", Journal of Computational Physics, **107**, pp. 262-281.
- [26] Hu, F. Q., 2001, "A stable, Perfectly Matched Layer for linearized Euler equations in unsplit physical variables", Journal of Computational Physics, **173**, pp. 455-480.
- [27] Hu, F. Q., 2005, "A Perfectly Matched Layer absorbing boundary condition for the Euler equations with a non-uniform mean flow", Journal of Computational Physics, **208**, pp. 469-492.
- [28] Lin, D. K., Li, X. D., and Hu, F. Q., 2011, "Absorbing boundary condition for nonlinear Euler equations in primitive variables based on the Perfectly Matched Layer technique", Computers & Fluids, **40**, pp. 333-337.
- [29] Tyler, J. M., and Sofrin, T. G., 1962, "Axial flow compressor noise studies", SAE Transactions, **70**, pp. 309-332.
- [30] Grace, S. M., Sondak, D. L., Eversman, W., and Cannamela, M. J., 2008, "Hybrid prediction of fan tonal noise", *AIAA paper 2008-2992*.
- [31] Cantrell, R. H., and Hart, R. W., 1964, "Interaction between sound and flow in acoustic cavities: mass, momentum and energy considerations", Journal of Acoustical Society of America, **36**, pp. 697-706.
- [32] Hu, F. Q., Kocaogul, I., and Li, X. D., 2012, "On the adjoint problem in duct acoustics and its solution by the Time Domain Wave Packet method", *AIAA paper 2012-2247*.

#### **List of Figures**

- **Figure 1**: Schematics for a time signal of a sinusoidal wave (left) and a wave packet (right). A wave packet has a shorter time duration compared to that of a sinusoidal wave, and thus is more efficient in time domain simulations. A wave packet also contains a broad range of frequencies.
- Figure 2: Illustration of Broadband Acoustic Test Pulse time function  $\Psi(t)$  and its spectrum, given in (4). The width of the spectrum can be controlled by parameter  $\omega_0$ .
- **Figure 3**: Instantaneous Contours for an acoustic source located inside the jet, showing shear layer effects on the radiation of sound. Left: without suppression, showing the growth of Kelvin-Helmholtz instability wave; Right: with Time Domain Wave Packet method, obtained by FFT of the time domain solution at the given frequency.
- **Figure 4**: Pressure contour history for the Time Domain Wave Packet method. Left: without instability wave suppression,  $\varepsilon = 0$ ; Right: with source filtering suppression technique,  $\alpha = 0.25$ ,  $\beta = 0.75$ .
- Figure 5: Pressure along y = 15, 50, and x = 100 for the Benchmark Problem shown in Figure 4. Solid lines are the computation by TDWP method and circles are the analytical solution.
- **Figure 6**: Schematics showing the variation of hub-to-tip ratio *h* and mean flow Mach number *M* along the SDT flow path. Top: Variation of hub-to-tip ratio; Bottom: Variation of the mean flow Mach number.
- Figure 7: A schematic of Time Domain Wave Packet method for duct radiation computation. Source mode is introduced at the source plane. The radiated sound propagates through the exhaust shear layer to the far field. Suppression of the instability wave by source filtering technique is turned on after the front of the wave packet has propagated through the shear layer. As the propagation of duct modes is dispersive (Dispersion relation of a duct mode is also shown above), waves with higher frequencies arrive at the far field sooner than those with lower frequencies. Here  $\omega_0$  denotes the minimum cut-on frequency and  $\omega_1$ ,  $\omega_2$ ,  $\omega_3$ , etc., indicate schematically a sequence of increasing frequencies.
- **Figure 8**: Computational domain and mesh for time domain simulation. Every fifth grid lines are shown. Two zones of body fitted finite element meshes are used, with Perfectly Matched Layer at all non-reflecting boundaries.
- **Figure 9**: Left: At approach condition, 61.7% of design speed, the dispersion relations show 5 cut-on radial modes at 2BPF when hub-to-tip ratio h = 0.529, M = 0.35. Right: The dispersion relations show 4 cut-on radial modes at 2BPF when hub-to-tip ratio h = 0.609, M = 0.4.
- Figure 10: Top: Sample pressure time history at a far field point, showing that the higher the frequency the earlier the arrival time, and the limiting frequency is  $\omega_0$  as indicated in the dispersion relation curve shown in Figure 7. Here,  $\omega_1$ ,  $\omega_2$ ,  $\omega_3$ , etc., indicate schematically a sequence of increasing frequencies. Bottom: FFT of the

time signal shown in the top figure, showing the cut-off phenomenon of the duct mode propagation as indicated in Figure 9. Mode number (-10,1).

- **Figure 11**: Time history of pressure at a sample point inside the shear layer of the exhaust flow. Top: without suppression; Bottom: with source filtering suppression technique.
  - **Figure 12**: Near-field pressure distribution (real part), mode (-10,0) and (-10,1) at 2BPF.
  - **Figure 13**: Near-field pressure distribution (real part), mode (-10,2) and (-10,3) at 2BPF.
  - **Figure 14**: Near-field pressure distribution (real part), mode (-10,4) at 2BPF.
- **Figure 15**: Experimental (circle) and computed (square) Sound Pressure Level in dB (ref.  $20\mu$  Pa) for the exhaust radiation, where angle is measured from the inlet forward. The modal power levels used for the computation are  $W_0 = 97(dB)$ ,  $W_1 = 61(dB)$ ,  $W_2 = 86(dB)$ ,  $W_3 = 91(dB)$  and  $W_4 = 52(dB)$  (ref.  $10^{-12}$ Watts).

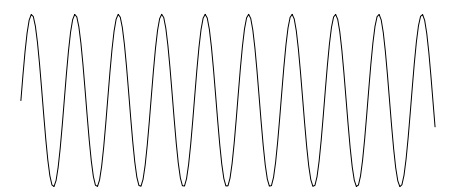




Fig. 1. Schematics for a time signal of a sinusoidal wave (left) and a wave packet (right). A wave packet has a shorter time duration compared to that of a sinusoidal wave, and thus is more efficient in time domain simulations. A wave packet also contains a broad range of frequencies.

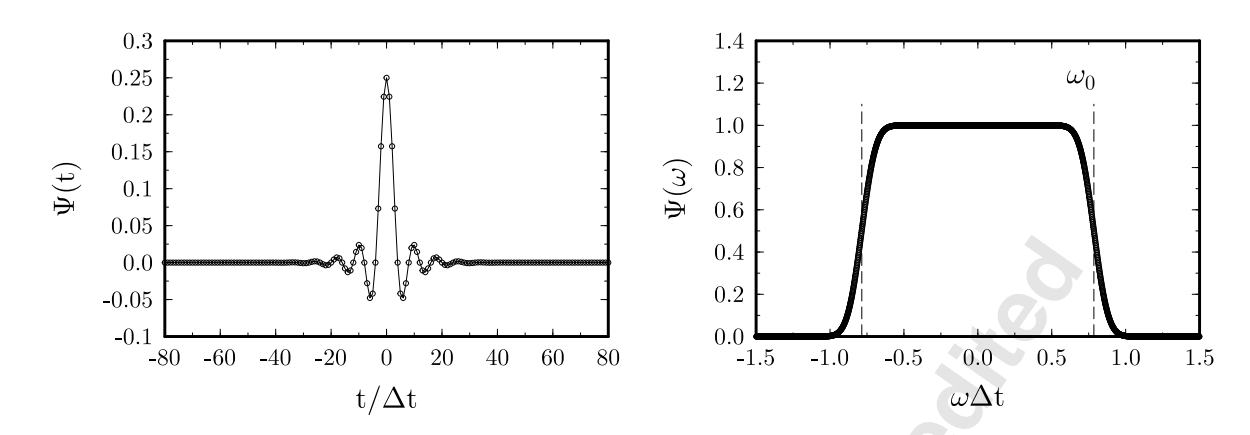
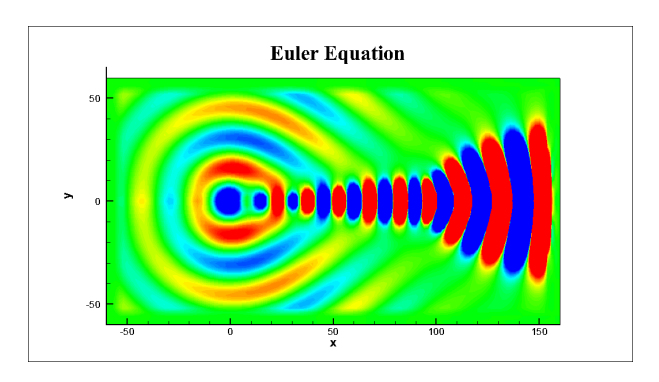


Fig. 2. Illustration of Broadband Acoustic Test Pulse time function  $\Psi(t)$  and its spectrum, given in (4). The width of the spectrum can be controlled by parameter  $\omega_0$ .



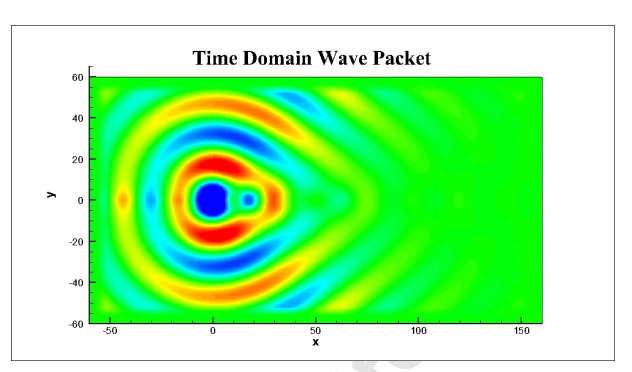


Fig. 3. Instantaneous Contours for an acoustic source located inside the jet, showing shear layer effects on the radiation of sound. Left: without suppression, showing the growth of Kelvin-Helmholtz instability wave; Right: with Time Domain Wave Packet method, obtained by FFT of the time domain solution at the given frequency.

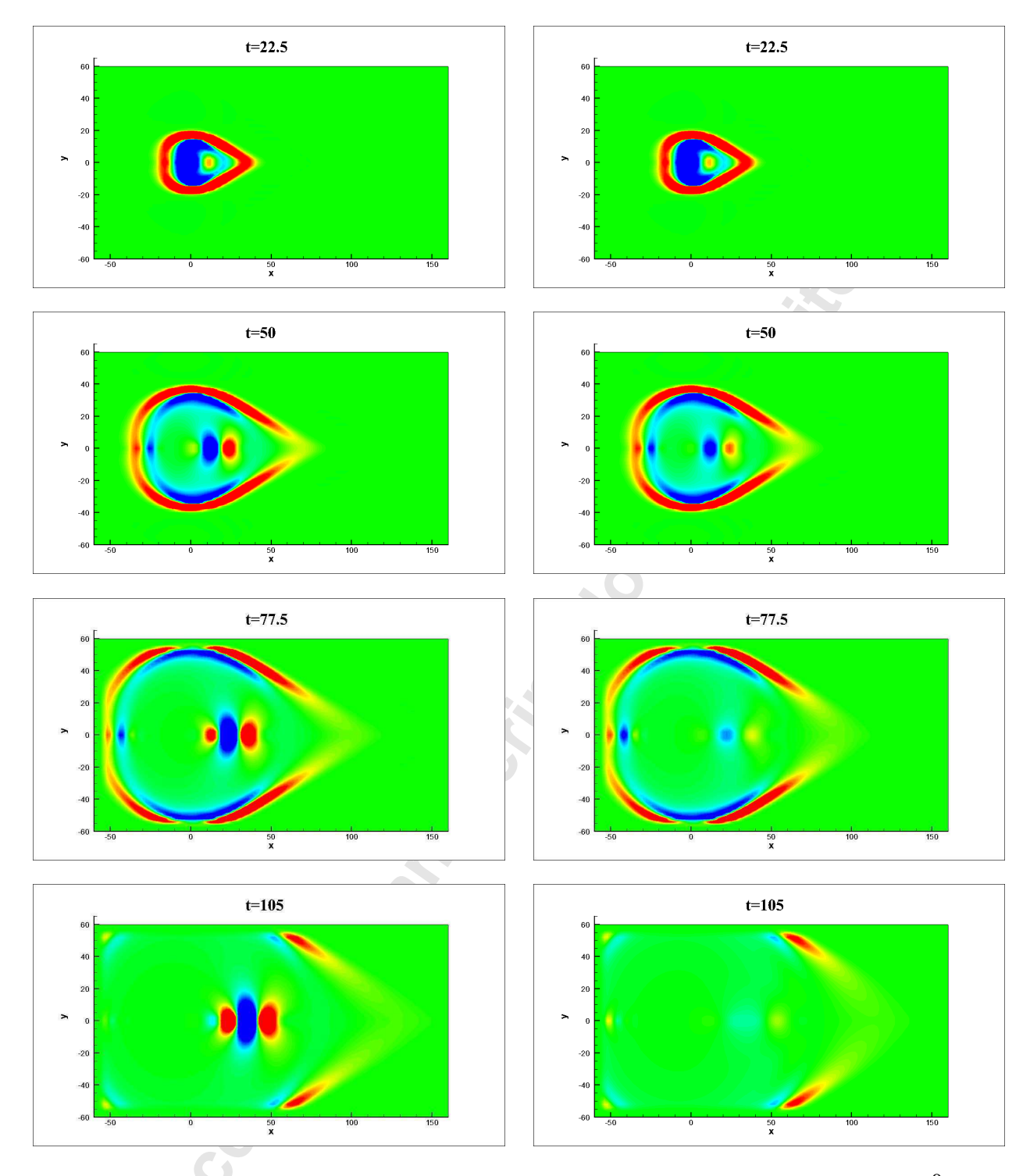


Fig. 4. Pressure contour history for the Time Domain Wave Packet method. Left: without instability wave suppression,  $\epsilon=0$ ; Right: with source filtering suppression technique,  $\alpha=0.25,\,\beta=0.75.$ 

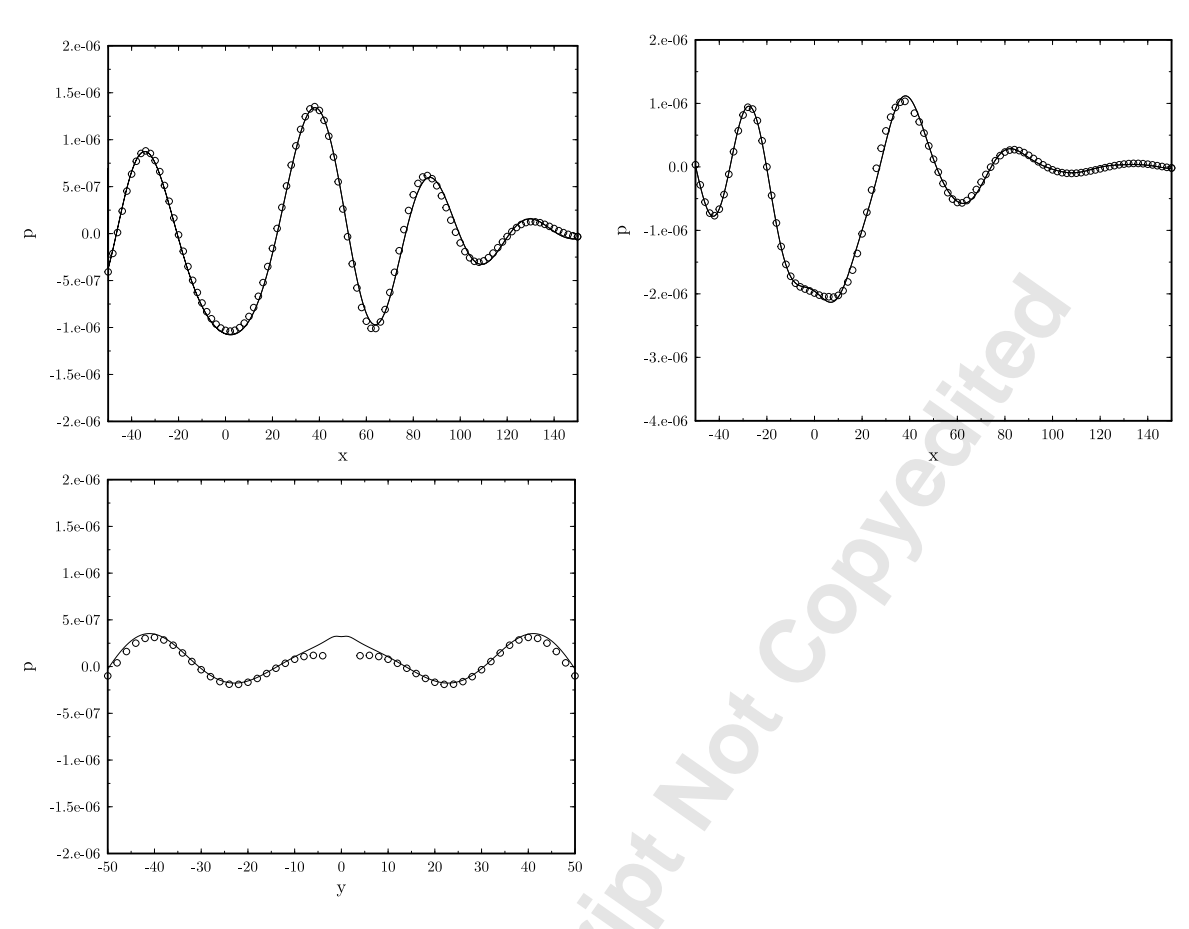


Fig. 5. Pressure along y = 15, 50, and x = 100 for the Benchmark Problem shown in Figure 4. Solid lines are the computation by TDWP method and circles are the analytical solution.

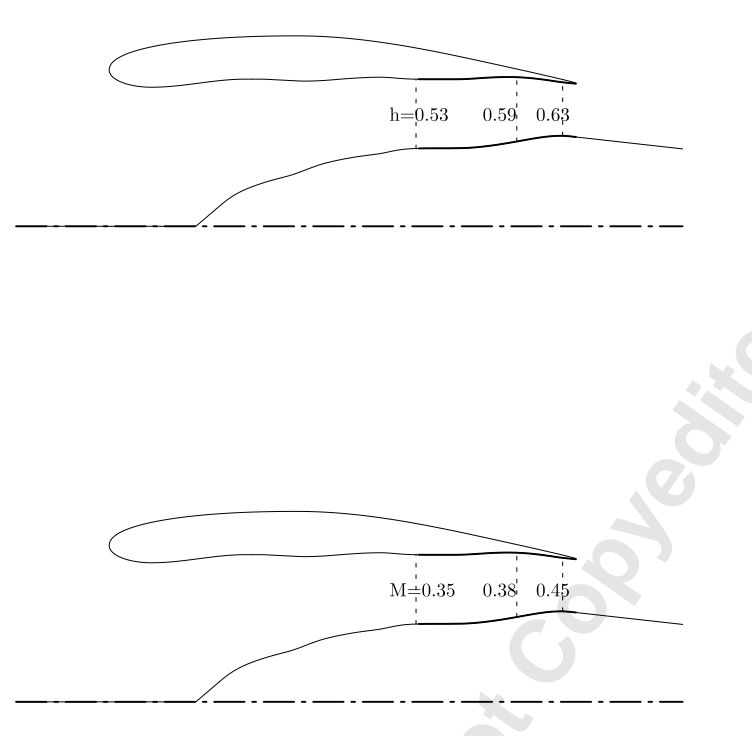


Fig. 6. Schematics showing the variation of hub-to-tip ratio h and mean flow Mach number M along the SDT flow path. Top: Variation of hub-to-tip ratio; Bottom: Variation of the mean flow Mach number.

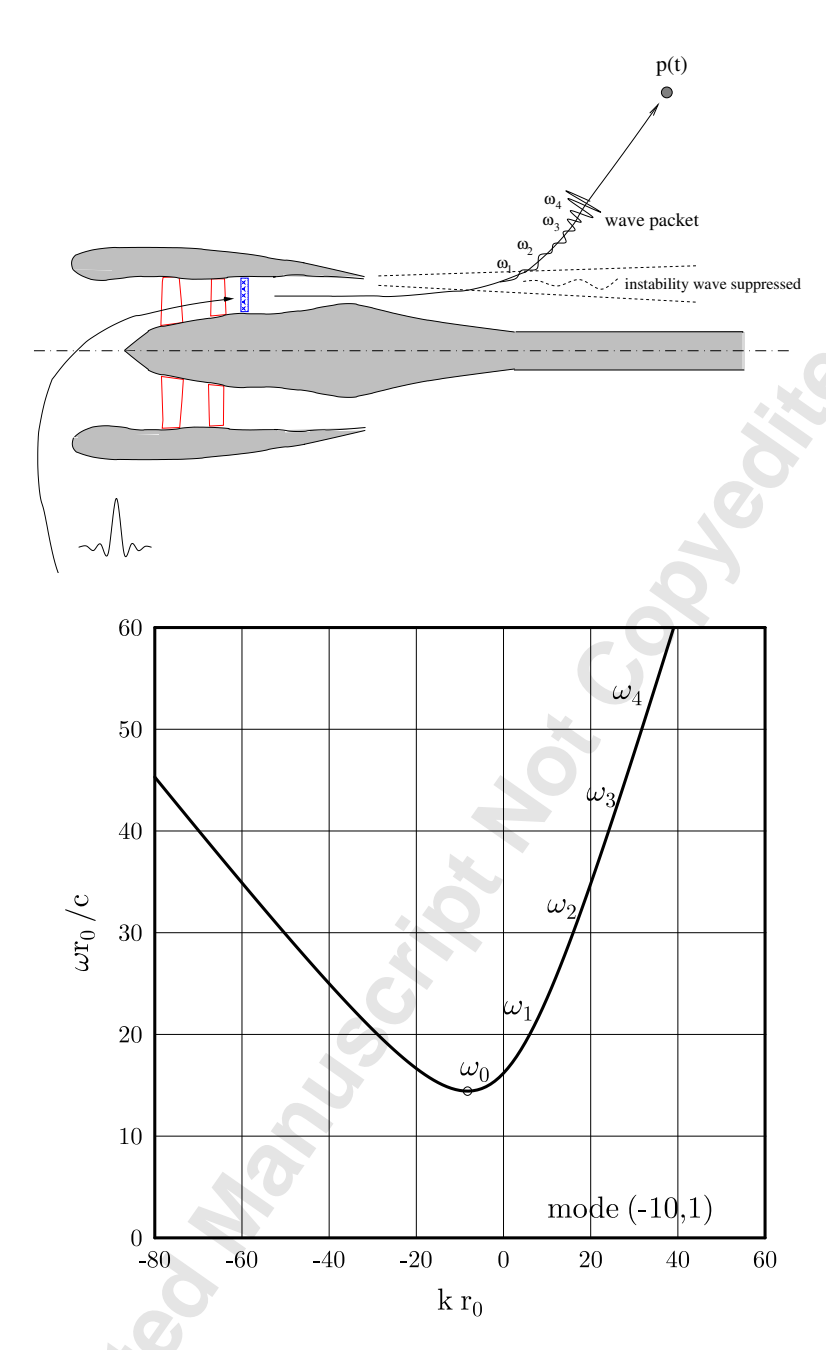


Fig. 7. A schematic of Time Domain Wave Packet method for duct radiation computation. Source mode is introduced at the source plane. The radiated sound propagates through the exhaust shear layer to the far field. Suppression of the instability wave by source filtering technique is turned on after the front of the wave packet has propagated through the shear layer. As the propagation of duct modes is dispersive (Dispersion relation of a duct mode is also shown above), waves with higher frequencies arrive at the far field sooner than those with lower frequencies. Here  $\omega_0$  denotes the minimum cut-on frequency and  $\omega_1$ ,  $\omega_2$ ,  $\omega_3$ , etc., indicate schematically a sequence of increasing frequencies.

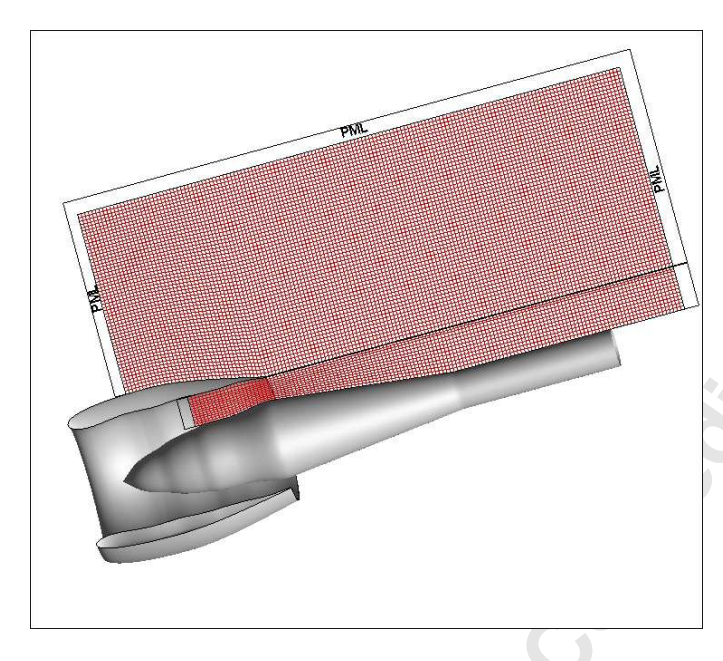


Fig. 8. Computational domain and mesh for time domain simulation. Every fifth grid lines are shown. Two zones of body fitted finite element meshes are used, with Perfectly Matched Layer at all non-reflecting boundaries.

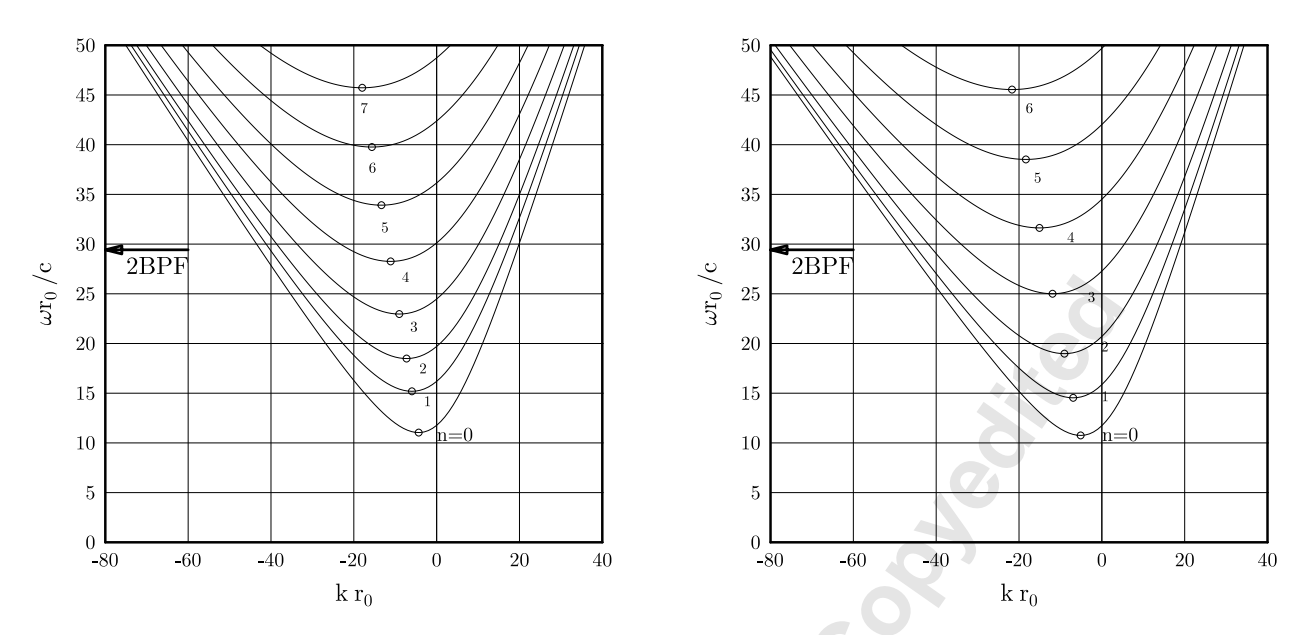


Fig. 9. Left: At approach condition, 61.7% of design speed, the dispersion relations show 5 cut-on radial modes at 2BPF when hub-to-tip ratio  $h=0.529,\,M=0.35$ . Right: The dispersion relations show 4 cut-on radial modes at 2BPF when hub-to-tip ratio  $h=0.609,\,M=0.4$ .

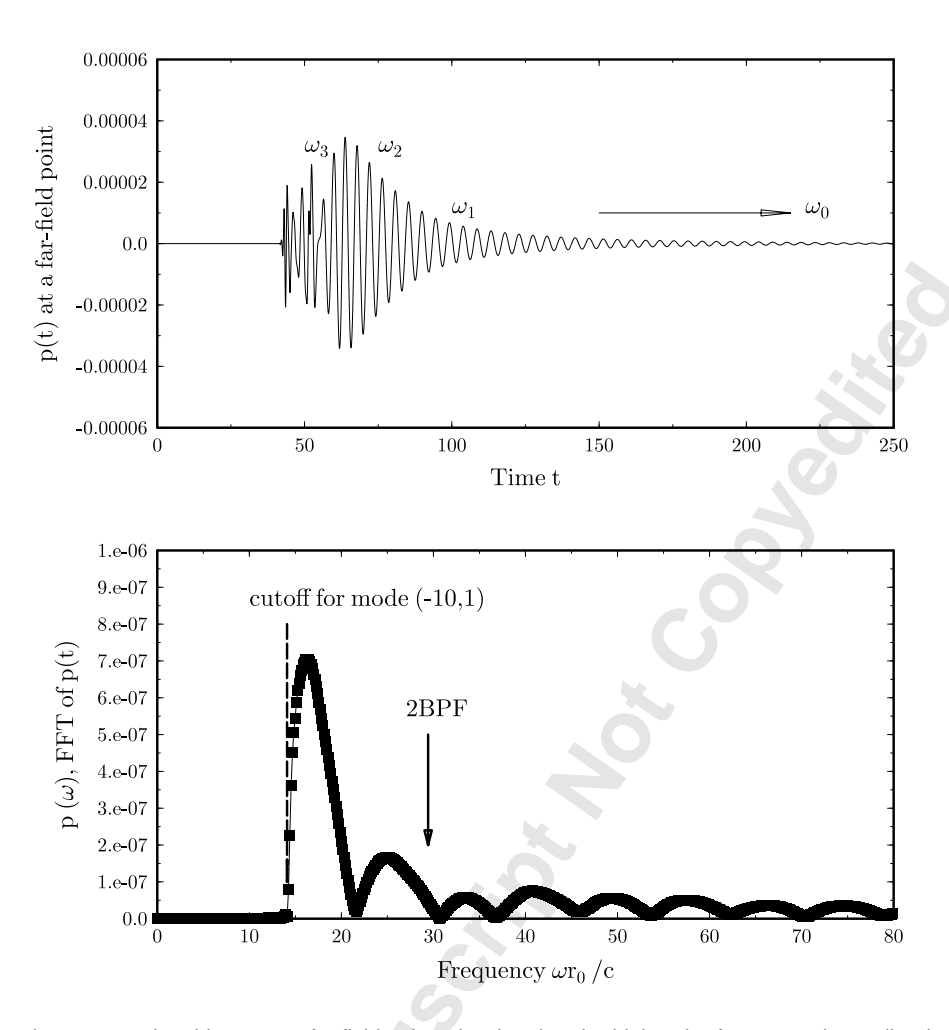


Fig. 10. Top: Sample pressure time history at a far field point, showing that the higher the frequency the earlier the arrival time, and the limiting frequency is  $\omega_0$  as indicated in the dispersion relation curve shown in Figure 7. Here,  $\omega_1$ ,  $\omega_2$ ,  $\omega_3$ , etc., indicate schematically a sequence of increasing frequencies. Bottom: FFT of the time signal shown in the top figure, showing the cut-off phenomenon of the duct mode propagation as indicated in Figure 9. Mode number (-10,1).

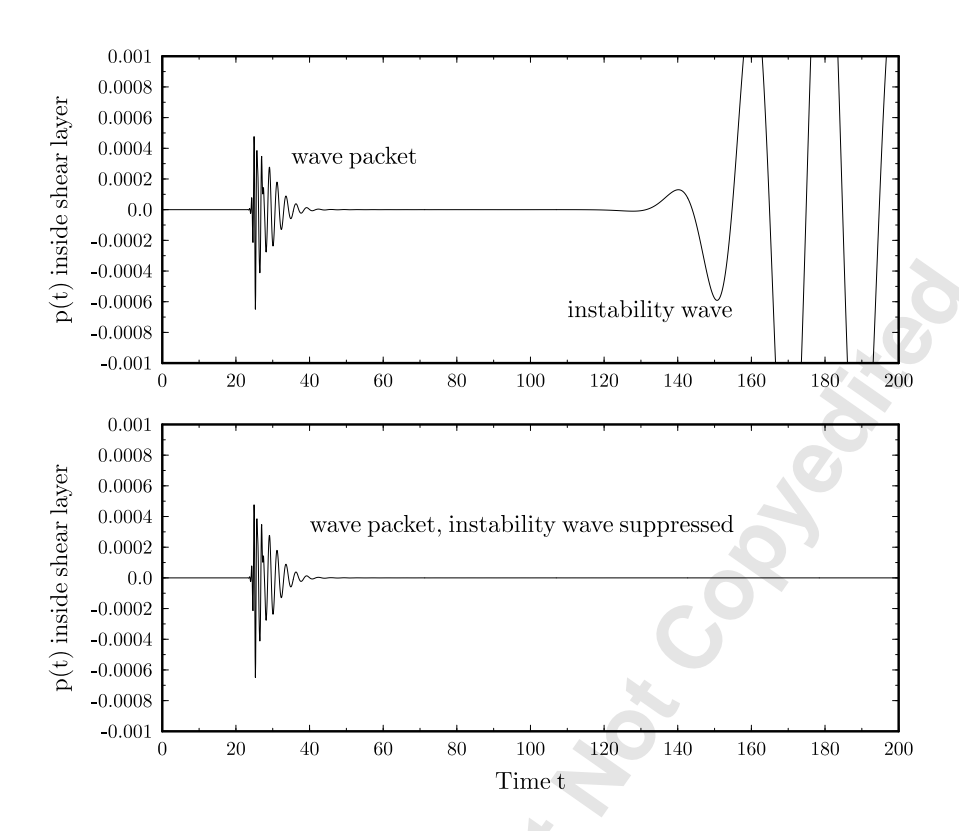


Fig. 11. Time history of pressure at a sample point inside the shear layer of the exhaust flow. Top: without suppression; Bottom: with source filtering suppression technique.

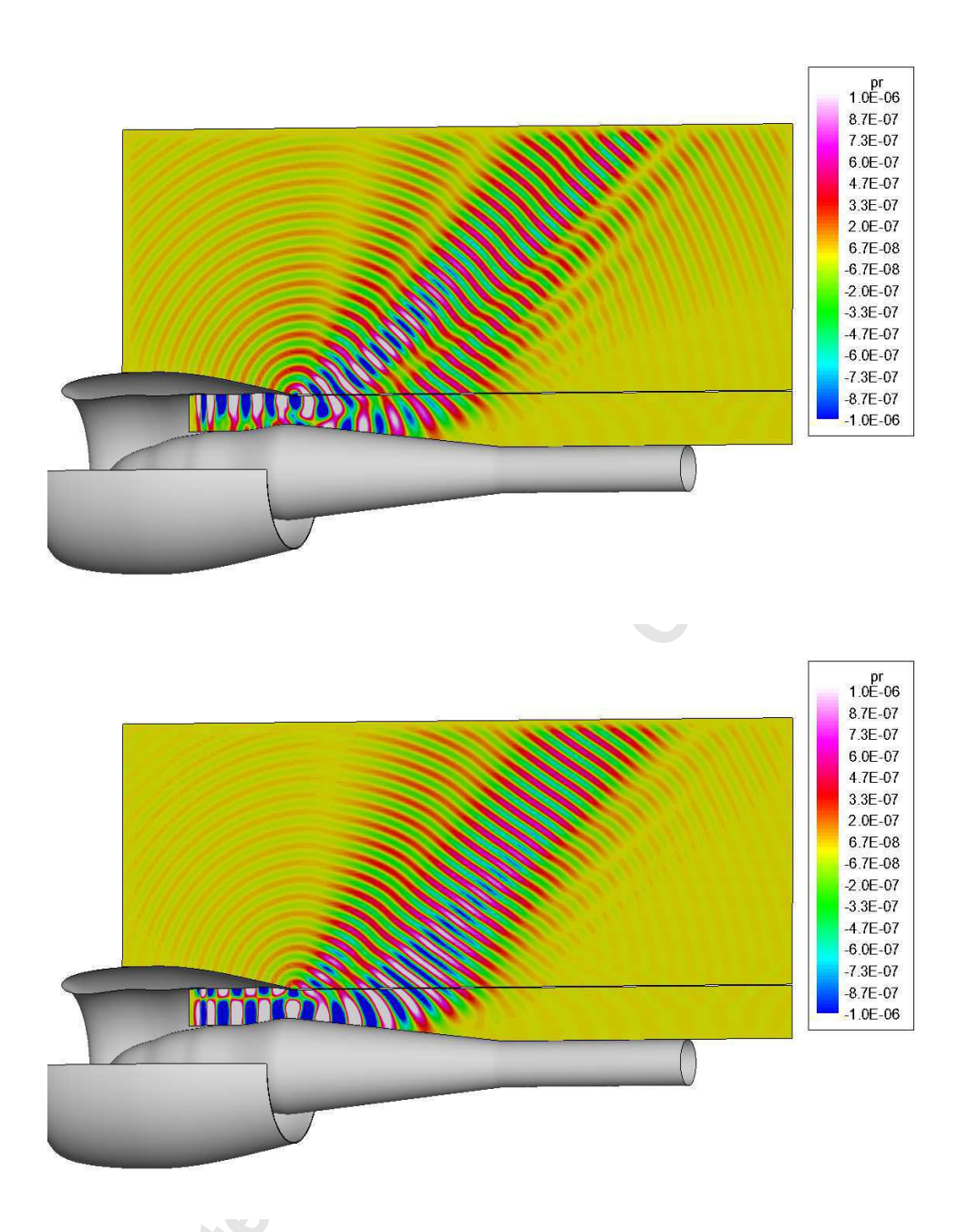


Fig. 12. Near-field pressure distribution (real part), mode (-10,0) and (-10,1) at 2BPF.

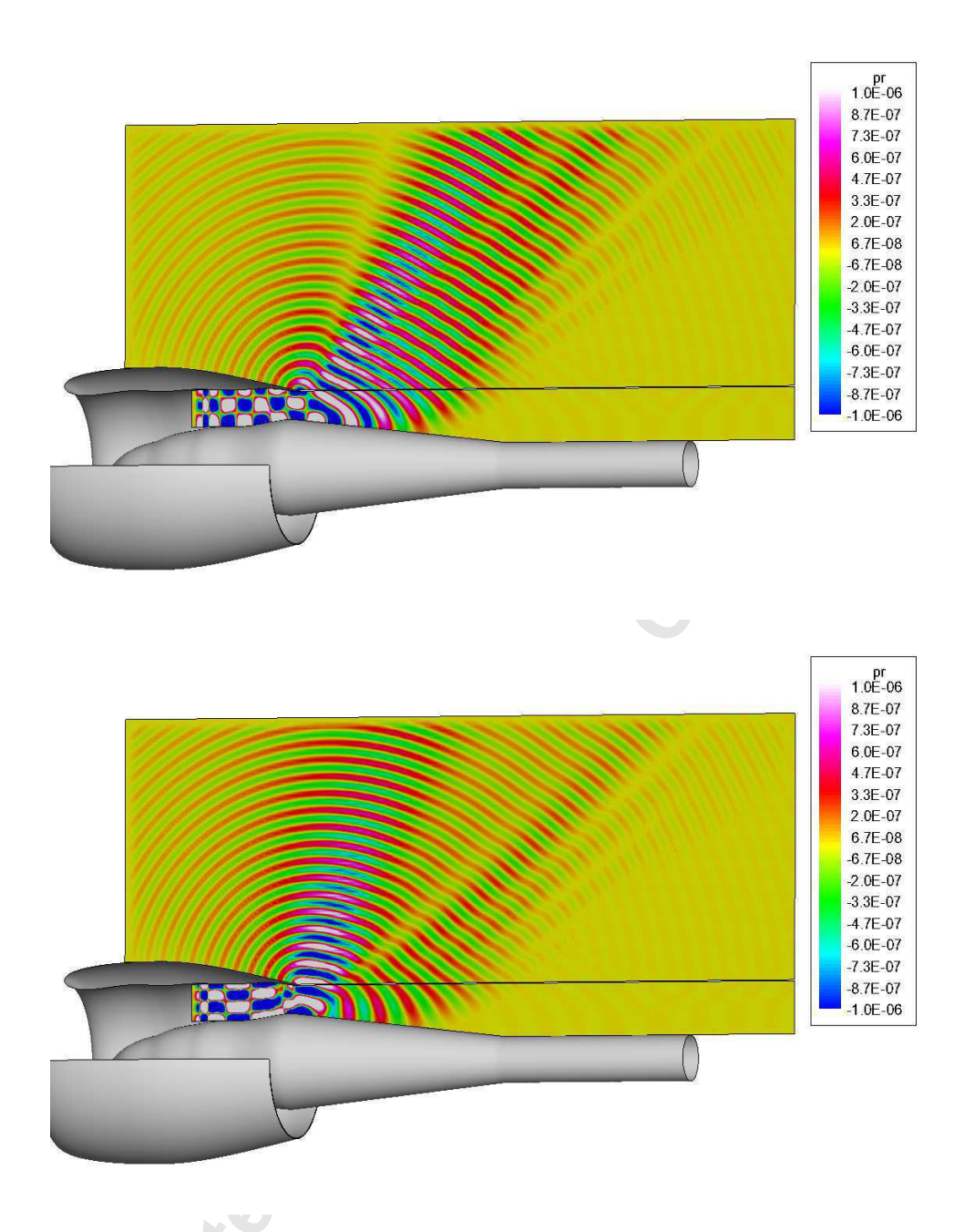


Fig. 13. Near-field pressure distribution (real part), mode (-10,2) and (-10,3) at 2BPF.

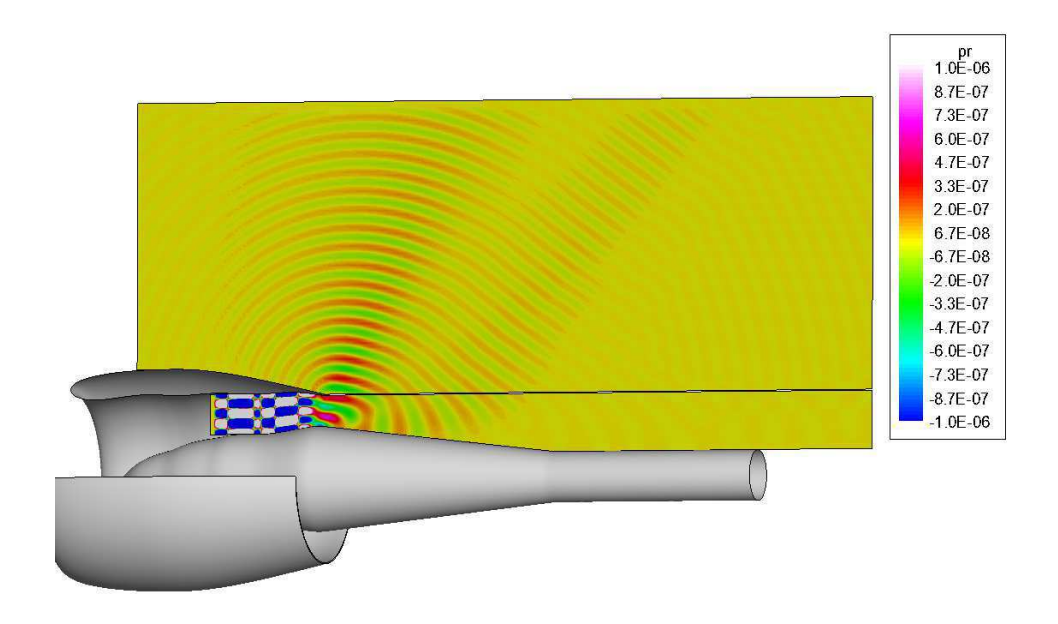


Fig. 14. Near-field pressure distribution (real part), mode (-10,4) at 2BPF.

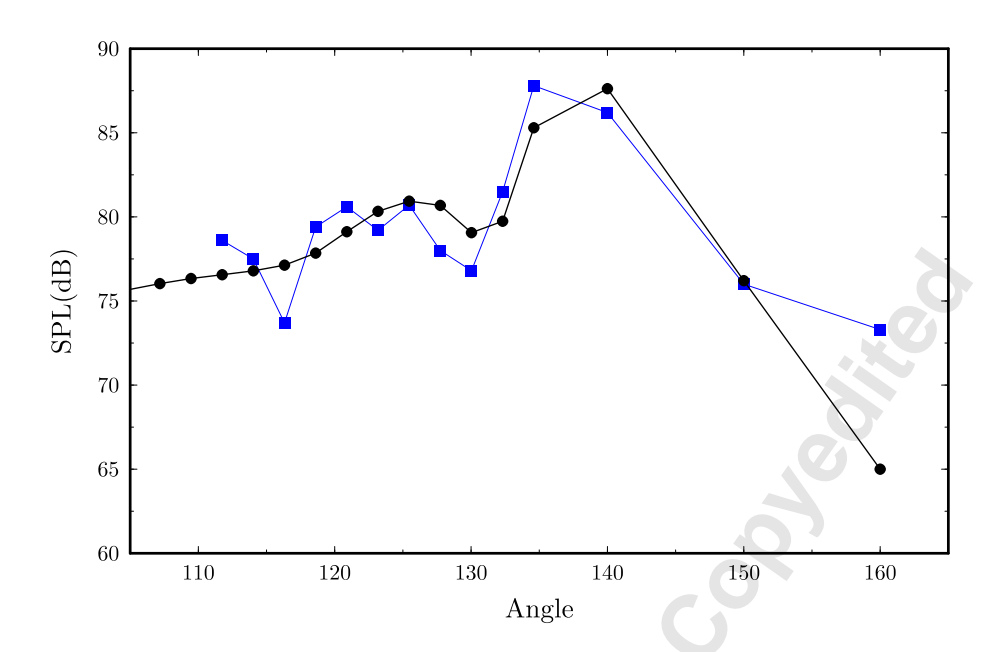


Fig. 15. Experimental (circle) and computed (square) Sound Pressure Level in dB (ref.  $20\mu$  Pa) for the exhaust radiation, where angle is measured from the inlet forward. The modal power levels used for the computation are  $W_0=97(dB)$ ,  $W_1=61(dB)$ ,  $W_2=86(dB)$ ,  $W_3=91(dB)$  and  $W_4=52(dB)$  (ref.  $10^{-12}$ Watts).